A new material constant of DNA is the major determinant of looping dynamics

Georgii Pobegalov[2], Maxim I. Molodtsov[*,2,3] and Bhavin S. Khatri[*,1,2]

[1] Department of Life Sciences, Imperial College London,
Silwood Park, Ascot, SL5 7PY, United Kingdom
[2] The Francis Crick Institute, 1 Midland Road, London, NW1 1AT, United Kingdom
[3] Dept of Physics & Astronomy, University College London,
Gower Street, London, WC1E 6BT, United Kingdom

*To whom correspondence should be addressed; E-mail: m.molodtsov@ucl.ac.uk,
bkhatri@imperial.ac.uk

DNA bending and looping is crucial for gene expression[1,2], packaging[3], and chromatin organization[4–7]. While the static flexibility of DNA is well-characterised by the bending elasticity or persistence length[8,9], no equivalent quantity related to how quickly it responds to external mechanical or thermal forces has to date been characterised. Here, by analysing the single molecule fluctuations of DNA several kilobases long, and by developing new theory for bending dissipation in semiflexible polymers, we show that DNA bending dynamics cannot be explained by friction between DNA and the solvent alone and requires significant contribution of intramolecular DNA friction. This defines a new material constant of DNA — the bending friction constant — which we determined to be $\zeta_B = 241 \pm 17\mu$g nm^3/ms. This magnitude corresponds to bending friction dominating dynamics of short DNA — up to ≈ 420nm or 1.24kbp — and a characteristic persistence time of DNA shapes of ≈ 1.2ms. Using these values, our theory accurately predicts measured spontaneous looping times[10,11] without any fitting parameters in stark contrast to the prevailing theory based only on solvent friction with DNA[12,13], which underestimates these times by 1,000-fold. Our measurement of DNA bending friction is also insensitive to changes in electrostatic screening suggesting that it is related to the local and complex energy barriers due to Watson-Crick base-pairs, base-stacking[14,15] and their interaction with water molecules[16–18] as DNA bends; this localised nature suggests an opportunity for biology to use specific sequence motifs to tailor the friction response of DNA. These findings change our understanding of DNA bending dynamics and highlight the nature of the fundamental trade-off between the speed limit for DNA bending by spontaneous fluctuations, versus the energy cost of manipulating DNA by enzymes, as necessitated by biological function and ultimately, natural selection.

Introduction

DNA is amongst the most important polymers in biology, as it stores the genetic code and the instructions for life. In addition to its role in information storage, its material and mechanical properties — in particular, how it loops and bends — play an intimate role in how that information is read-out in the process of transcription initiation[1,2], how it becomes packed as chromatin as it wraps around nucleosomes[3], how the genome is organised in eukaryotes[4–6] or packed within the tight confines of a viral capsid[19]. In these processes, the persistence length or bending elasticity of DNA determines the equilibrium shape of DNA in response to external mechanical constraints or forces. However, what is missing from a full characterisation of the mechanical properties of DNA is how quickly DNA changes shape in response to external mechanical forces and constraints. To date models of DNA dynamics assume that the only source of dissipation to retard its motion, comes from Stoke's friction with the solvent[12,13], where energy is lost through the numerous random interactions with water molecules. Yet, since the earliest investigations of the physics of polymers, it has been tacitly understood that this assumption is only true in the limit of long polymers — known as Kuhn's theorem[20,21] — and that for sufficiently short polymers, dissipation is dominated by energy lost through internal friction due to internal energy barriers to local motion within the polymer. On sufficiently small length scales, we expect the dynamics of DNA to be determined by intramolecular bending friction that slows down DNA motion; higher friction leads to slower dynamics.

Intramolecular nternal friction originates from energy barriers to local changes in shape (Fig.1) and it has been studied for locally flexible polymers such as synthetic polymers[21–25], polysaccharides[26,27], proteins[28–31] and ssDNA[32]. Just as we can measure the overall, or end-to-end, elastic properties of molecules in single-molecule experiments — for example from force-extension experiments[8] — we can also measure their effective end-to-end friction, usually from analysis of the power spectrum of their fluctuations[26] or from the out-of-phase response to oscillatory forcing[33,34]. There are two key signatures of local intramolecular friction in single-molecule experiments: 1) an increasing end-to-end friction with decreasing contour length and 2) an increasing end-to-end friction for increasing tension[27]. Both effects arise because the friction is related to how quickly the chain can respond to perturbations[27]: smaller chain lengths[21] and chains at high stretch — where the chain entropy has been massively reduced — have fewer degrees of freedom available to respond and so this slows the response and is manifested as an increased effective friction.

Surprisingly, the intramolecular bending friction, for one of the most important biological molecules — DNA — has not been measured and therefore, how it contributes to the DNA dynamics in essential biological processes remains unknown. As described in Fig.1, although DNA is often idealised as a simple elastic rod, where the only source of dissipation would be from the solvent, DNA is a molecule with complex internal structure with a potentially complex energy landscape for bending, which may come from local energy barriers due to interactions between the numerous atoms in DNA itself as well as interactions between the atoms of DNA and water molecules as DNA bends. By analysing the fluctuations of DNA for a range of contour lengths and tensions, we show the friction of DNA show both signatures for an intramolecular origin, discounting solvent friction as an explanation. We thereby quantify a new material constant of DNA — the bending friction — from single molecule experiments, using a first principles theory of bending friction in semiflexible polymers, properly accounting for the role of tension, building on a previous heuristic approach[31]. Using our measurement of the bending friction constant, we then demonstrate that for a biologically important range of contour lengths and tensions, bending friction is the by-far the dominant contributor to DNA bending and looping dynamics.

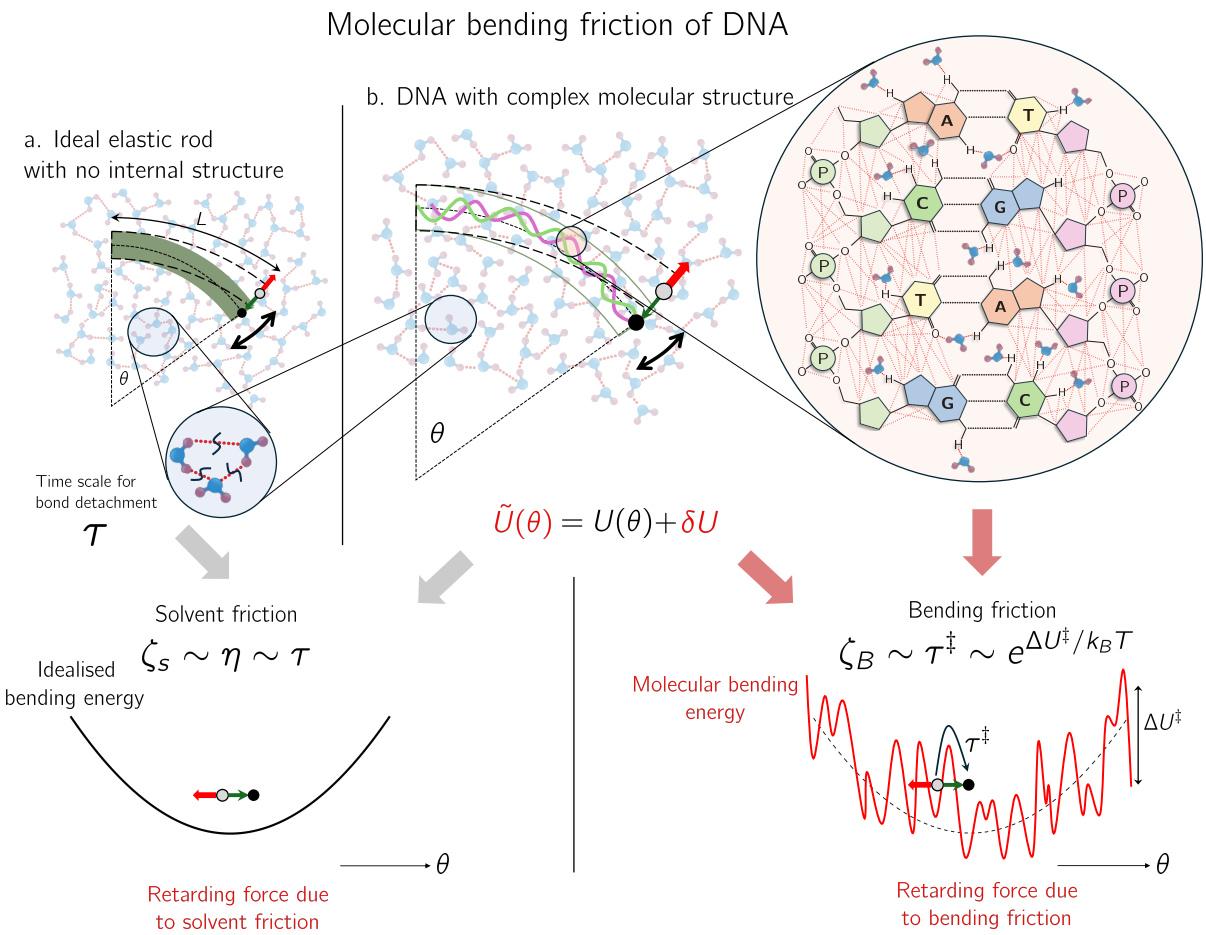

Figure 1: The origins of bending friction within DNA. a) an ideal elastic rod with no internal structure has a smooth quadratic elastic energy $U(\theta)$ as function of bend angle θ, where the curvature is controlled by the bending elasticity. The grey dot moving to the black dot over time indicates a change in bend angle of the rod with the red arrow indicating the retarding frictional force. For the ideal rod friction ζ_s arises only from dissipation with the solvent, which depends on the viscosity of water η, which is an emergent property determined by the timescale τ of water hydrogen bond lifetimes. b) DNA segment: unlike an idealised elastic rod has a complex internal molecular structure. The total energy of DNA is made up from numerous local interactions, shown in red on right of the figure, as well as the main contributions from base-pairing and base stacking. As DNA bends, complex changes in the relative positions of all the atoms, gives a corresponding complex change in the energy of DNA. In addition, specific binding of water molecules to nucleotides, will necessitate unbinding and binding of water as DNA bends. These factors could give rise to rough energy landscape with local energy barriers, where $\Delta U^{\ddagger}/k_B T$ is the roughness of the energy landscape — on the scale of thermal energy $k_B T$ — to DNA bending due to local interactions in DNA, and ζ_B is the emergent bending friction of DNA due to local barrier hopping on timescale $\tau^{\ddagger}$.

Extracting DNA friction from fluctuations

To fill this gap in our knowledge and determine the role of bending friction in DNA dynamics, we devised an experiment schematically shown in Fig.2a. DNA is stretched to different mean forces F by appropriately choosing the distance between the two beads trapped in laser tweezers that

hold opposite ends of the DNA. We choose a force range of 1pN$\leq F \leq$ 5pN to be comfortably in the highly stretched regime at the lower force ($F \gg k_BT/\ell_P \approx 0.08$pN), and to avoid backbone stretching at the highest force. At each force the DNA molecule is held for 6s, while the time-series of fluctuations in each trap are recorded: $x_1(t)$ and $x_2(t)$ at sampling frequency of $\approx$ 78kHz. Example time series are shown in Fig.2b as a function of increasing force, showing the DNA chain is being stretched. From the length fluctuations $\ell(t) \sim x_2(t) - x_1(t)$, we calculate the velocity power spectrum $P_v(\omega)$ (VPSD) of the bead fluctuations at each force (Fig.2c) using the relation $P_v = \omega^2 P_\ell$, where $P_\ell(\omega)$ is the regular power spectrum. This results in weighting information towards higher frequencies and ultimately provides a more reliable measurement of DNA friction, since it is directly related to power dissipated per unit frequency, which increases at higher frequencies (see Extended Data Fig.1).

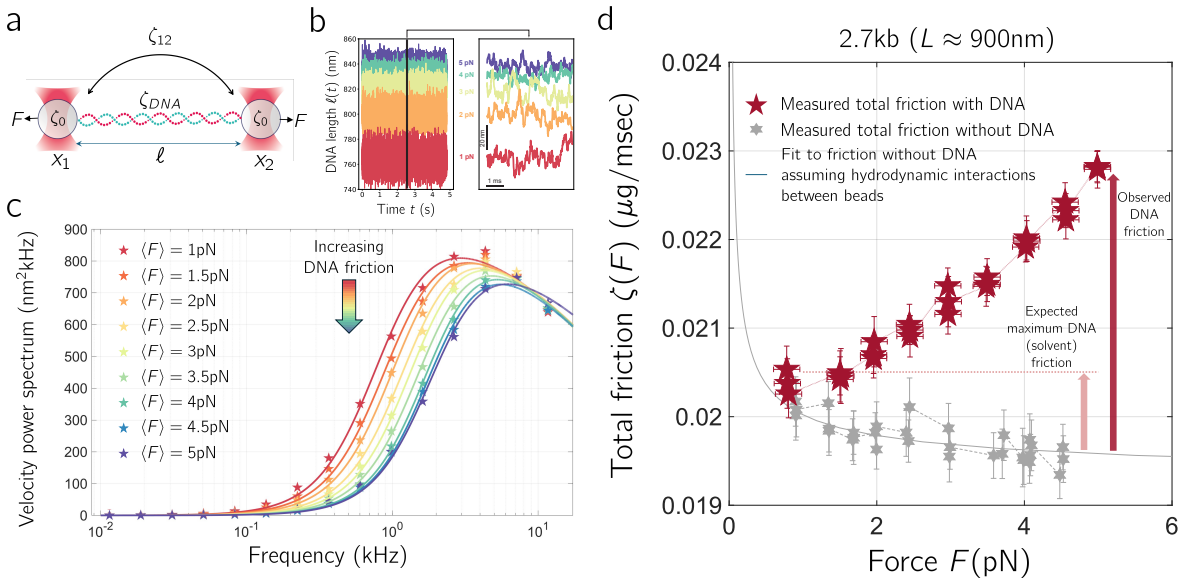

Figure 2: Measuring the friction response of DNA as a function of force. a) DNA is tethered between two beads at a mean force F using dual optical trap. The time-series of the position of each trap, $x_1(t)$ and $x_2(t)$, is recorded, where the dynamics of the system is determined by the friction of DNA ζ_{DNA}, the friction of each bead ζ_0 and the effective friction due to the hydrodynamic interactions between the beads, ζ_{12}: where the total friction $\zeta = \zeta_{DNA} + \frac{1}{2}(\zeta_0 + \zeta_{12})$ (Supplementary Information:Eqn.S17). b) Example time series of length $\ell(t)$ of 2.7kbp DNA as a function of force, showing increased extension for increasing forces. c) the velocity power spectrum (VPSD) of the fluctuations in b) describe distribution of dissipation across frequencies. The decrease in the peak height with the increasing tension can only be explained by increasing friction of DNA (Extended Data Fig.2). d) The total effective friction of the trap DNA system (red pentagrams) as a function of force. We see DNA friction increases above the background hydrodynamic friction (grey hexagrams — measured without DNA — and grey solid line, fit with hydrodynamic theory between two beads). This contrasts to the expectation if solvent friction were the only source of dissipation indicated by the dotted pink line, assuming DNA is completely stretched to its contour length ($\zeta_s = 2\pi\eta L/\ln(L/w)$; $L = 902.6$nm, $w = 2.4$nm). Vertical error bars on friction measurements are confidence intervals ($\approx$ 67%) from fits to VPSD, horizontal error bars are standard error estimates from calculating the mean force from the 6s time-series at each force ($n \approx 400,000$) combined with errors from force correction (Supplementary Information: section S6).

The velocity power spectrum is a function of two main force-dependent viscoelastic parameters of DNA: the end-to-end elasticity $\kappa_{DNA}(F)$ — which is the well characterised entropic elasticity often modelled by a WLC[8,9] — and the end-to-end friction of DNA $\zeta_{DNA}(F)$. Our data in Fig.2c shows that the velocity power spectrum is highly sensitive to changes in the average tension applied to DNA; as we demonstrate in the Extended Data Fig.2 the maximum value of the VPSD is inversely proportional to the friction constant of the system, which is a direct demonstration that the friction of DNA is increasing with increasing tension. Fitting to the velocity power spectrum at each force in Fig.2c, using a model of the velocity power spectrum that includes relevant corrections due to non-stationary effects of Brownian motion at high frequency (Supplementary Information: Eqn.S18), we determine the resulting friction constant of the bead, trap and DNA $\zeta(F)$ as a function of force shown in Fig.2d, as solid squares. Three main factors contribute to the total friction $\zeta(F)$: 1) the friction of DNA, $\zeta_{DNA}(F)$, which includes both solvent and bending friction, 2) the effective friction of each bead, ζ_0, and 3) the effective friction arising from interactions between the beads ζ_{12}. Although, the latter two have no explicit dependence on force, as DNA is stretched at increasing tensions, the separation between the beads increases, decreasing the contribution of the friction from background bead hydrodynamics. We measured the background hydrodynamics separately without DNA (Fig.2d, grey squares) showing that contributions 2) and 3) to the friction matches closely standard Oseen theory[35] given by the solid grey line (see Supplementary Information Eqn.S11 for details) and remains largely flat for the forces above 1.5 pN.

Our data show that in the presence of DNA, tethered between the beads, the friction constant increases approximately linearly with increasing force, over and above the background bead friction. This is in stark contrast to the expectation of an approximately constant friction of $\zeta_s \approx 0.00092\mu$g/ms for 2.7kb long DNA (dashed pink line in Fig.2d) at high stretch ($F \gg k_BT/\ell_P \approx 0.08$pN), due to solvent friction, where we assume DNA is a rod of length $L \approx 900$nm, and width $w = 2.4$nm[36,37]. Our data in Fig.2d show that friction increases with force and reaches approximately 0.0035μg/ms, above the background hydrodynamic friction, at $F = 5$ pN, which is almost four-times the expected solvent friction.

Our fitting also yields the elastic constant $\kappa(F)$, which matches the entropic elasticity expected of a WLC at high stretch (Extended Data Fig.3). The fit of the VPSD data also accounts for the effective frequency-dependent mass of water entrained around each bead, which should be independent of force, which we verify in Extended Data Fig.4.

Force-dependent friction from semiflexible polymer dynamics with bending friction

Because solvent friction alone could not explain the linear increase in friction of DNA with force, we sought to rationalise our findings by modifying the standard model of semiflexible polymer dynamics with tension F at high stretch ($F \gg k_BT/\ell_P \approx 0.8$pN). This describes DNA as idealised elastic rod whose shape fluctuates dynamically due to Bronwian motion and friction with the solvent. We propose that due to internal frictional processes within DNA there will be local bending dissipation proportional to the rate of change of local curvature. As we describe in the Methods, calculating the local forces due to this dissipation gives rise to a modified equation for semiflexible polymer dynamics for a Dissipative Worm-Like Chain (DWLC) under tension (Eqn.4).

Our aim is to evaluate the additional, or excess, end-to-end friction of the chain, as a function of tension F, due to bending dissipation, over and above hydrodynamic solvent contributions or Stokes' friction of DNA (see Methods). We do this by analysing Eqn.4 using standard normal mode analysis, and evaluating the relevant moments to calculate the autocorrelation function of the

chain. The end-to-end excess friction is then calculated from the derivative of the autocorrelation function[38] to give the following, in the limit of the chain at high force/stretch (valid for forces $F > 0.08$pN):

$$\Delta\zeta_{DNA}(F) = \frac{\sqrt{2}\tilde{\zeta}_s^{1/4}\zeta_B^{3/4}}{k_B T L} F. \tag{1}$$

This shows that explicit inclusion of the bending friction in the equations of motion leads to the linear increase of the friction coefficient with external force (Fig.2d). Note that the friction of the dissipative WLC is inversely proportional to the contour length L, which is classic signature of internal dissipation in polymers[21,39]. Thus, DNA friction that takes into account internal bending dissipation increases for shorter DNA.

A new material constant of DNA

Having established the theoretical description of bending friction using the DWLC model, we can now infer its value from the experimental data. As we expect to see an increasing friction due to bending dissipation in DNA to be inversely proportional to contour length, we measure a number of single molecules of DNA for lengths between 2.7kbp and 8.8kbp ($\approx$ 900nm$\leq$ 3000nm). We determine the excess DNA friction, $\Delta\zeta_{DNA}(F)$, as the residual friction over and above the background friction — due to the hydrodynamic interactions between beads (grey pentagrams in Fig.2d) — and hydrodynamic (Stokes) solvent friction of DNA— which we expect is approximately constant at high stretch — and fit this data using Eqn.1, which has a single fitting parameter ζ_B, with the other parameters being known quantities. With DNA, the hydrodynamic interactions between the beads and DNA are likely to be complex and the various contributions to the background hydrodynamic friction non-additive, so for simplicity we use a fitting constant multiplying the background friction measured without DNA (grey solid line Fig.2d) to subtract out this background to give the excess friction in Fig.3a; as the effects of DNA solvent friction are independent of tension at these forces, this fitting constant automatically removes this contribution. As expected this fitting parameter should be near to 1, which we verify is indeed the case in Extended Data Fig.5.

The resulting measurements of the excess DNA friction for all lengths (various colours), with the effective background bead and DNA solvent friction removed are shown in Fig.3a. The fitting of Eqn.1 to our data shows that our DWLC model accounts for the main unexpected feature of the data: a linear increase of the excess DNA friction with increasing force. In addition, Fig.3a clearly shows that as the contour length decreases the excess friction increases, which is in qualitative agreement with Eqn.1; in Extended Data Fig.6, we additionally plot the normalised friction $L\Delta\zeta_{DNA}$ as a function of force and demonstrate very good quantitative agreement with $\Delta\zeta_{DNA} \sim \frac{1}{L}$. Thus, experimentally observed excess friction is fully explained by the bending friction of DNA.

In stark contrast to the observed data, if the excess solvent friction were due to solvent friction — i.e. our assumption of solvent friction contributions not being constant — we plot the expected contribution in Fig.3b, which as discussed would be independent of the applied tension for the force ranges used and increases with increasing contour length.

Furthermore, to test whether internal DNA bending friction depends on the electrostatic interactions in the DNA, we compared experiments performed at physiological salt concentrations (in PBS buffer) with experiments carried out under very low salt conditions (1 mM, in Hepes buffer; see Methods). This comparison (closed and open data circles, respectively, in Fig.3a) shows no dependence of the bending friction on the salt concentration. For each molecule in these experiments we also performed force-extension measurements and extracted their persistence length. As expected and in the agreement with previous studies[40–43], we observed an increase in the persistence length

for the low salt buffer (Supplementary Information: section S3).

These experiments show that bending friction is a material constant of DNA independent of the buffer conditions in our experiments. Therefore, we determined a quantitative value for the bending friction constant of DNA, ζ_B, by combining all data. To this end, we fit the data in Fig.3 using Eqn.1 for each buffer condition and each length independently, which gives rise to the value of ζ_B at each contour length and buffer; accounting for finite-size effects[44] (Extended Data Fig.6), we find $\zeta_B = 238 \pm 20\mu$g nm^3/ms for the PBS buffer and $\zeta_B = 249 \pm 32\mu$g, for the low salt Hepes buffer. Although there is a modest increase in the mean bending friction, there is no statistically significant difference in the bending friction constant due to electrostatic screening (assuming normal distribution of errors on fit parameter, we used a two-sided z-test to give p-value: $p = 0.77$). We take the variance-weighted average to give our final value of $\zeta_B = 241 \pm 17\mu$g nm^3/ms (s.e.m). This supports our hypothesis that the origin of the excess DNA friction we measure is due to local bending dissipation rather than long-range electrostatic interactions.

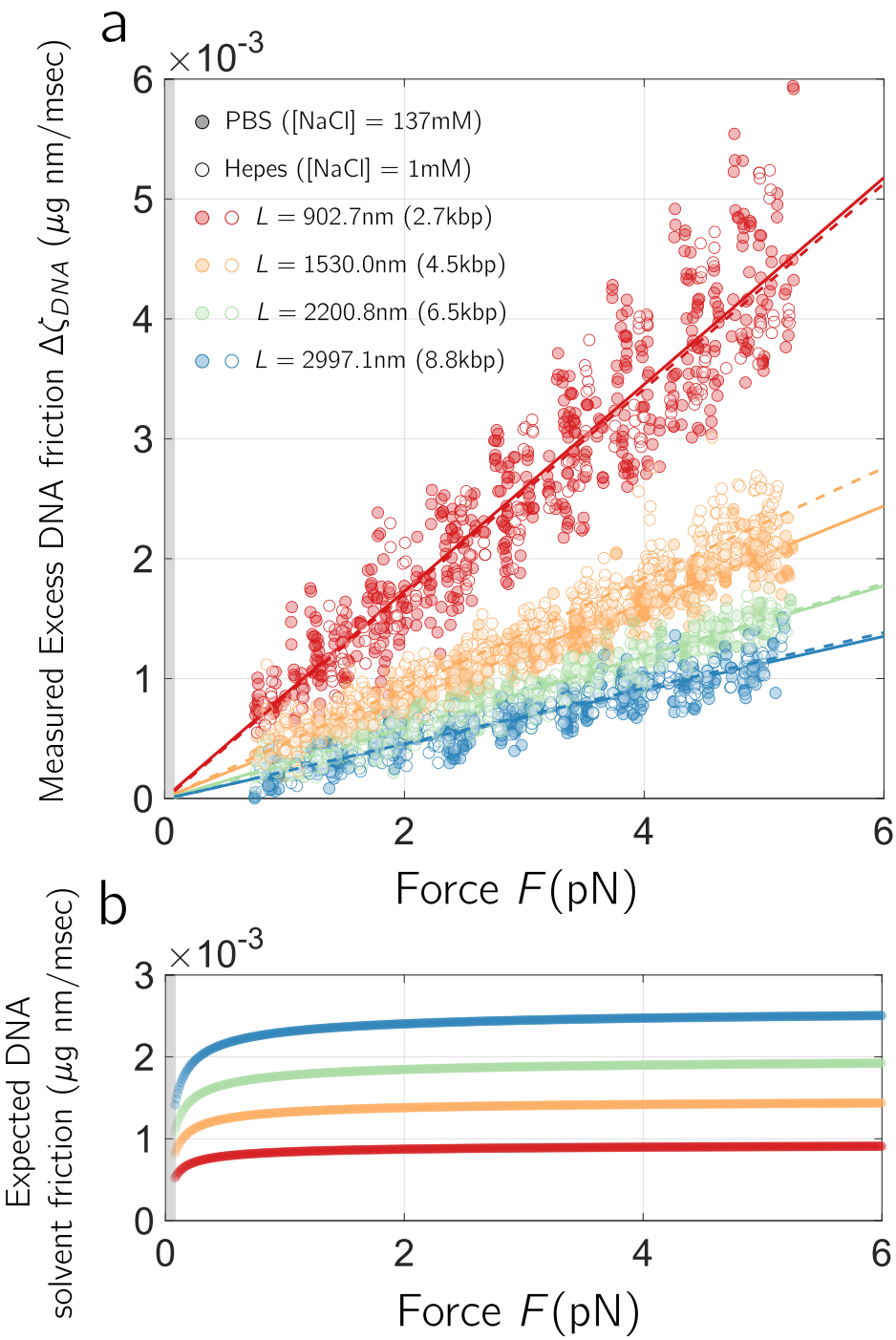

Figure 3: a) The measured excess end-to-end friction of DNA as a function of force showing linearity and increasing friction for decreasing contour length as predicted by Eqn.1. Closed circles are in normal PBS buffer and open circles are in the low salt Hepes buffer. The data is fit using Eqn.1 with single fitting parameter ζ_B, with $\tilde{\zeta}_s = 2\pi\eta/\ln(L/w)$ with fits shown with solid lines (PBS) or dashed lines (Hepes). The number of measurements on independent single molecules at each length and for each buffer condition are given in Table.2. b) The expected excess DNA friction, if it were due to solvent dissipation assuming DNA is highly stretched ($F > 0.08$pN) using $\zeta_s = 2\pi\eta\ell(F)/\ln(\ell(F)/w)$, where $\ell(F) = L\left(1 - \sqrt{\frac{k_B T}{4F\ell_P}}\right)$ is the extension of the WLC as a function of force F.

The dynamics of DNA looping on small length scales

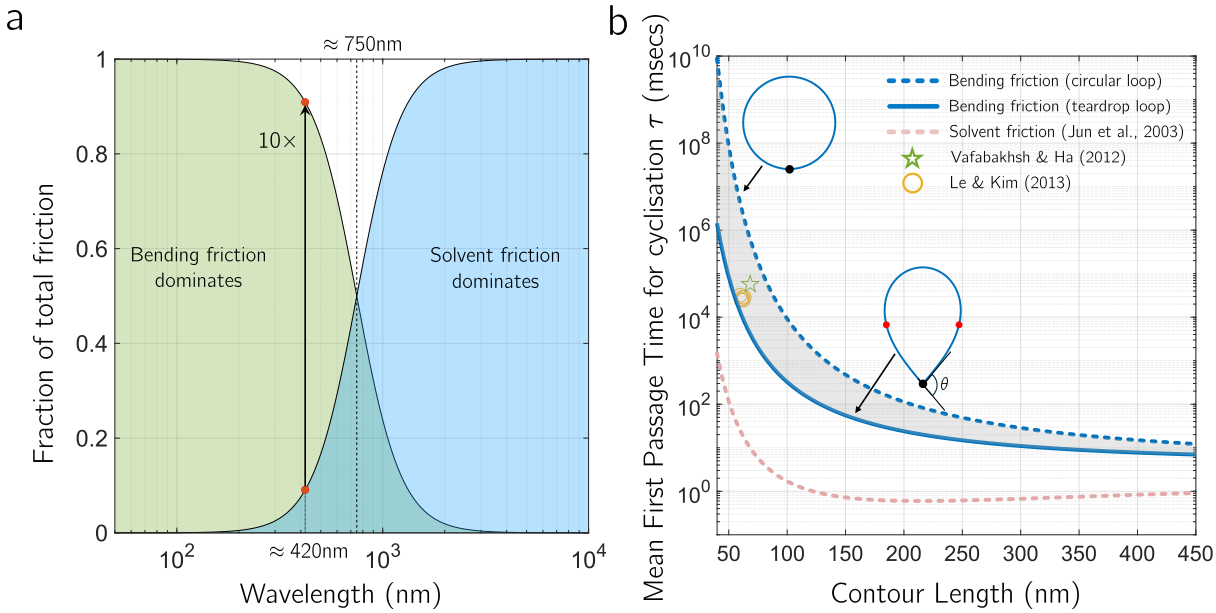

Figure 4: DNA dynamics on small length scales. a) Relative contribution of bending and solvent friction to total mode friction for a given wavelength. b) Plot of mean first passage times (MFPT) for DNA loop closure as a function of contour length. The predictions based on the theory developed in this paper for circular loops (Eqn.3) and minimum energy tear-drop loops (Supplementary Information: section S5), where bending friction and bending energy dominate, are shown as dashed blue line and solid blue line, respectively. While the prediction based on a WLC with only solvent dissipation[12] is shown by the dashed pink line. Experimental measurements of MFPT using cyclisation assays are shown by open circles[11] and open pentagrams[10].

We have determined a new fundamental material constant for DNA, ζ_B which determines how DNA locally dissipates energy as it bends and loops. With our measurement of ζ_B we can now calculate relative contributions of solvent and bending friction for any DNA length at zero force. The normal mode analysis using (Eqn.5) shows that the critical lengthscale at which solvent and bending contributions to the friction are equal at zero external force is $L^* \approx 750$nm (Fig.4a) (see also Supplementary Information: section S4), which is equivalent to a DNA length of approximately 2.2kbp. This also shows that for DNA contour lengths $L \leq 420$nm, solvent friction is $10\times$ smaller than bending friction; in other words we can model the spontaneous dynamics of DNA, considering only the contributions from bending friction, for contour lengths up to about $9\ell_p$. On the other hand, for very small contour lengths — up to about a persistence length — it is likely DNA kinking plays a role in DNA flexibility and dynamics[45]. Therefore, we expect bending friction dominates for DNA lengths $\ell_P \leq L \leq 9\ell_P$ and have significant contributions up to $15\ell_P \rightarrow 20\ell_P$. One important consequence of this is that as we will show below, the dynamics of DNA is greatly simplified in the regime where bending friction dominates, as we can in many cases reduce its description to a one-dimensional Langevin/Smoluchowski equation for the DNA curvature.

In this regime, we can calculate the average time it takes for DNA to completely change shape, which we will call persistence time of DNA. In the absence of external force and in the limit that bending friction dominates, all modes relax with the same characteristic time $\tau_n = \frac{\zeta_B}{\kappa_B}$ independent

of mode number n, which implies that the overall persistence time of the DNA shapes will simply be

$$\tau_P = \frac{\zeta_B}{\kappa_B}. \tag{2}$$

Given the value of ζ_B that we have determined, and assuming $\kappa_B = k_B T \ell_P \approx 200\text{pNnm}^2$ this gives a persistence time of $\tau_P = 1.2\text{ms}$. In other words, in the absence of external force for DNA where bending friction dominates, its shape completely changes under thermal fluctuations in approximately 1.2 ms.

Although, the contribution of bending friction decreases with the increasing length of DNA, it also increases with the increasing external tension. At zero external force, bending friction stops playing significant role for DNAs longer than 750nm. However, as Eqn.1 shows, at sufficiently large tension, once the chain is highly stretched, the effects of bending friction can manifest at much longer contour lengths, for which at zero tension they would be too weak to play a role in dynamics. Indeed we have taken advantage of this to extract the bending friction from DNA up to 8.8kb long, which in the absence of external force would be too small to detect (Extended Data Fig.7).

Comparison to the time to cyclisation of DNA

Cyclisation assays have become the standard way to estimate the rate of loop closure of DNA [10,11], the characterisation of which is important to a understanding the dynamics of number of DNA looping processes in molecular biology. Current theory to calculate mean first passage times are based on semiflexible polymer dynamics without bending friction [12,13] and are consequentially complex calculations as they require consideration of the different dynamics of all the modes of the polymer. However, when bending friction dominates solvent friction and in the limit that bending energy dominates the chain entropy, we can make the assumption that the DNA conformation is roughly an arc of a circle with curvature $\Gamma = 1/R$, where R is the radius of this circle. The resulting stochastic dynamics is then the standard Smoluchowski equation for a single degree of freedom, the curvature Γ, with effective friction $\zeta_\Gamma = L\zeta_B$ and bending energy $U(\Gamma) = \frac{L}{2}\kappa_B\Gamma^2$. Using standard flux-over population method and Kramer's approximations (see Supplementary Information: section S5 for details) we find the mean first passage time (MFPT) τ^* for loop closure is:

$$\tau^* = \frac{\zeta_B}{\kappa_B}\sqrt{\frac{L}{2\pi\ell_p}}e^{\frac{2\pi^2\ell_p}{L}}, \tag{3}$$

which is a pleasingly simple closed-form expression, compared to the theory of Jun et. al [12] for a WLC where the only dissipation is with the solvent, which is more complicated to evaluate. This calculation is valid, when $L \ll (2\pi)^2\ell_p \approx 2000\text{nm}$ and so this approximation should be reasonably accurate for all lengths for which bending friction dominates ($L < 420\text{nm}$).

However, experiments measuring the time for loop closure of DNA [46], suggest that it is most likely to adopt — at least initially — a tear-drop conformation, where the ends come together with zero curvature and a non-zero angle θ between the end tangent vectors (Fig.4b) . Previous theoretical work, shows the minimum energy conformation corresponds to $\theta \approx 100^\circ$ [47] and an overall energy which is roughly 70% the energy of a circular loop [47,48]. As the tear-drop conformation has lower energy than a circular one, we expect that Eqn.3 will be an overestimate of the mean first passage time, when comparing to the loop closure experiments we discuss below. As we show in the Supplementary Information (section S5), we can make a simple estimate of the time for

closure of a tear-drop loop, when bending friction and bending elasticity dominate, by making the assumption that the MFPT will be dominated by a portion of the chain around its midpoint where the curvature is highest, which are indicated by the red circles in Fig.4b.

In Fig.4b we compare the predictions of MFPT for loop closure of DNA between our theory, for circular and tear-drop loops, and the theory in which the only source of dissipation is the solvent (as represented by by Jun et al.[12]). For the bending dissipation theory we used the DNA bending friction we measured experimentally and plotted two limiting cases, one where DNA loops in a perfect circle, which requires higher energy and another one when DNA forms a tear-drop shape with minimal energy (Fig.4b). On the same plot we showed experimentally available looping times from Vafabakhsh & Ha[10] and Le & Kim[11], for DNA length between $60 - 70$nm. We see that our theory agrees with the data, which lies between the lower bound set by the tear-drop loop closure theory and upper bound by the circular loop closure theory; in contrast, we see that the theory accounting for only solvent friction massively underestimates the looping time by approximately 1,000-fold.

Discussion

A key question remains: what is the underlying origin of bending friction within DNA? Our experiments in buffers with different ionic strength suggest that the role of long-range electrostatic interactions are weak—for example, from the negatively charged backbone of DNA — since the bending friction constant in our experiments is insensitive to changing salt concentrations and the strength of electrostatic screening. Therefore, we postulate that the origin must be in local and potentially complex energy barriers that dynamically constrain DNA as it bends; it is plausible that as DNA bends, there will be a very large number of (microscopically distinguishable) ways that all atoms change their positions that give rise to the same approximate bend angle of DNA, and the complexity of those interactions would give rise to a local roughness in the energy landscape, as indicated in Fig.1. The two main potential sources of such barriers are hydrogen bonding between base-pairs and base stacking interactions, so as DNA bends the relative orientation and position of the base-pairs will change, which could lead to complex interactions between the numerous atoms with consequent local intermediate barriers.

An alternative, or additional contributing factor, as depicted in Fig.1, is the binding and unbinding of water molecules to DNA base-pairs through the major and minor grooves, which could give rise to an effective energy barrier to bending, since the water molecules will need to rearrange as DNA bends. It is well known that there is a hydration spine of ordered water molecules populating the minor groove and less ordered waters within the major groove[16,17], which could decrease the local mobility of DNA bending. In particular, simulations suggest water can bind more specifically by hydrogen bonding to DNA bases — for example, bridging interactions between adenine and thymine bases — that induce stabilities of order $3k_BT$[18]; as DNA bends the geometry of the minor and major grooves will change and these specifically bound water molecules have to rearrange, potentially traversing energy barriers of order or greater than $3k_BT$ and contributing to the bending friction of DNA.

Recent genome-wide studies of the "bendability" of DNA have shown that this measure of local DNA flexibility can vary across the genome[49]. However, these loop-seq cyclisation assays are based on 50bp to 100bp segments of DNA, where kinking[45] likely makes a significant contribution. For longer lengths of DNA, above the persistence length, for which our bending friction theory applies, the localised nature of bending friction suggests that there may be a dependence on specific sequence; for example, how water molecules rearrange when DNA bends likely depends on

the local base pairing. Single and dinucleotide motifs could give rise to a local friction response, and an opportunity for DNA dynamics to be tailored by natural selection, beyond the bulk value we have measured in this paper. Clearly, our DNA loop-closure time predictions call for empirical measurements of loop-closure times for lengths greater than the persistence length and investigation of its sequence dependence.

Our finding of a new material constant of DNA, which we have shown is major determinant of its looping and bending dynamics, from roughly 1 to up to 9 persistence lengths, has very wide and important implications for the maximum speed and energy input of any process in molecular biology, where proteins, enzymes or molecular motors must manipulate, bend or loop DNA. At these lengths DNA looping is thought to be critical for initiating transcription in eukaryotes; for example, in vertebrates enhancer interactions with the promoter are thought to occur between 100-1000bp (30 and 300nm)[2,50]; above approximately 1 persistence length is the regime where bending friction will dominate the looping and cyclisation dynamics of transcription. Other important examples, where DNA looping on these lengths scales is important include the wrapping of DNA around histones[3] and the loop extrusion of DNA[51]. For all these molecular processes, being able to quantitatively predict looping times is important to determine whether such processes can arise spontaneously by Brownian motion or require activated burning of ATP to overcome bending dissipation to achieve the manipulation of DNA more quickly, as necessitated by biological function, and ultimately natural selection.

References

[1] Elizabeth M. Blackwood and James T. Kadonaga. Going the Distance: A Current View of Enhancer Action. *Science*, 281(5373):60–63, 1998.

[2] Anil Panigrahi and Bert W. O'Malley. Mechanisms of enhancer action: the known and the unknown. *Genome Biology*, 22(1):108, 2021.

[3] Timothy J. Richmond and Curt A. Davey. The structure of DNA in the nucleosome core. *Nature*, 423(6936):145–150, 2003.

[4] Natalia Naumova, Maxim Imakaev, Geoffrey Fudenberg, Ye Zhan, Bryan R. Lajoie, Leonid A. Mirny, and Job Dekker. Organization of the Mitotic Chromosome. *Science*, 342(6161):948–953, 2013.

[5] Tatsuya Hirano. Condensin-Based Chromosome Organization from Bacteria to Vertebrates. *Cell*, 164(5):847–857, 2016.

[6] Frank Uhlmann. SMC complexes: from DNA to chromosomes. *Nature Reviews Molecular Cell Biology*, 17(7):399–412, 2016.

[7] Job Dekker and Leonid A. Mirny. The chromosome folding problem and how cells solve it. *Cell*, 187(23):6424–6450, 2024.

[8] C Bustamante, JF Marko, ED Siggia, and S Smith. Entropic elasticity of lambda-phage DNA. *Science*, 265(5178):1599–1600, 1994.

[9] John F Marko and Eric D Siggia. Stretching DNA. *Macromolecules*, 28(26):8759–8770, 1995.

[10] Reza Vafabakhsh and Taekjip Ha. Extreme Bendability of DNA Less than 100 Base Pairs Long Revealed by Single-Molecule Cyclization. *Science*, 337(6098):1097–1101, 2012.

[11] Tung T. Le and Harold D. Kim. Measuring Shape-Dependent Looping Probability of DNA. *Biophysical Journal*, 104(9):2068–2076, 2013.

[12] S. Jun, J. Bechhoefer, and B.-Y. Ha. Diffusion-limited loop formation of semiflexible polymers: Kramers theory and the intertwined time scales of chain relaxation and closing. *Europhysics Letters*, 64(3):420–426, 2003.

[13] Peter J. Mulligan, Yi-Ju Chen, Rob Phillips, and Andrew J. Spakowitz. Interplay of Protein Binding Interactions, DNA Mechanics, and Entropy in DNA Looping Kinetics. *Biophysical Journal*, 109(3):618–629, 2015.

[14] A A Travers. The structural basis of DNA flexibility. *Philosophical Transactions of the Royal Society of London. Series A: Mathematical, Physical and Engineering Sciences*, 362(1820):1423–1438, 2004.

[15] Alexandra Balaceanu, Diana Buitrago, Jürgen Walther, Adam Hospital, Pablo D Dans, and Modesto Orozco. Modulation of the helical properties of DNA: next-to-nearest neighbour effects and beyond. *Nucleic Acids Research*, 47(9):4418–4430, 2019.

[16] Mary L. Kopka, Albert V. Fratini, Horace R. Drew, and Richard E. Dickerson. Ordered water structure around a B-DNA dodecamer A quantitative study. *Journal of Molecular Biology*, 163(1):129–146, 1983.

[17] Ahmed M. Rozza, Imre Bakó, and Julianna Oláh. Theoretical insights into water network of B-DNA duplex with Watson-Crick and Hoogsteen base pairing geometries. *Journal of Molecular Liquids*, 362:119728, 2022.

[18] Chi H. Mak. Hydration Waters Make Up for the Missing Third Hydrogen Bond in the A·T Base Pair. *ACS Physical Chemistry Au*, 4(2):180–190, 2024.

[19] William M. Gelbart and Charles M. Knobler. Pressurized Viruses. *Science*, 323(5922):1682–1683, 2009.

[20] W. Kuhn and H. Kuhn. *Helv. Chim. Acta*, 28:1533, 1945.

[21] Pierre Gilles de Gennes. *Scaling Concepts in Polymer Physics*. Cornell University Press, 1985.

[22] Kunihiro Osaki and John L Schrag. Viscoelastk Properties of Polymer Solutions in High-Viscosity Solvents and Limiting High-Frequency Behavior. I. Polystyrene and Poly(-methylstyreste). *Polymer Journal*, 2(4):541–549, 1971.

[23] R. Cerf. Possible existence of two classes of conformational changes in linear polymeric chain molecules. *Chemical Physics Letters*, 22(3):613–615, 1973.

[24] Jacobus W M Noordermeer, John D Ferry, and Norio Nemoto. Viscoelastic Properties of Polymer Solutions in High-Viscosity Solvents and Limiting High-Frequency Behavior. III. Poly(2-substituted methyl acrylates). *Macromolecules*, 8(5):672–677, 1975.

[25] Masaru Kawakami, Katherine Byrne, Bhavin S Khatri, Tom C B McLeish, and D. Alastair Smith. Viscoelastic properties of single poly(ethylene glycol) molecules. *Chemphyschem*, 7(8):1710–1716, Aug 2006.

[26] M. Kawakami, K. Byrne, B.S. Khatri, T. C. B. Mcleish, S. E. Radford, and D. A. Smith. Viscoelastic properties of single polysaccharide molecules determined by analysis of thermally driven oscillations of an atomic force microscope cantilever. *Langmuir*, 401:400–403, 2004.

[27] Bhavin S Khatri, Masaru Kawakami, Katherine Byrne, D. Alastair Smith, and Tom C B McLeish. Entropy and barrier-controlled fluctuations determine conformational viscoelasticity of single biomolecules. *Biophys J*, 92(6):1825–1835, Mar 2007.

[28] Anjum Ansari, Colleen M. Jones, Eric R. Henry, James Hofrichter, and William A. Eaton. The Role of Solvent Viscosity in the Dynamics of Protein Conformational Changes. *Science*, 256(5065):1796–1798, 1992.

[29] Alessandro Borgia, Beth G Wensley, Andrea Soranno, Daniel Nettels, Madeleine B Borgia, Armin Hoffmann, Shawn H Pfeil, Everett A Lipman, Jane Clarke, and Benjamin Schuler. Localizing internal friction along the reaction coordinate of protein folding by combining ensemble and single-molecule fluorescence spectroscopy. *Nature communications*, 3:1195, 2012.

[30] David de Sancho, Anshul Sirur, and Robert B Best. Molecular origins of internal friction effects on protein-folding rates. *Nature Communications*, 5, 2014.

[31] Bhavin S Khatri, Katherine Byrne, Masaru Kawakami, David J Brockwell, D. Alastair Smith, Sheena E Radford, and Tom C B McLeish. Internal friction of single polypeptide chains at high stretch. *Faraday Discuss*, 139:35–51; discussion 105–28, 419–20, 2008.

[32] Milad Radiom, Mark R Paul, and William A Ducker. Dynamics of single-stranded DNA tethered to a solid. *Nanotechnology*, 27(25):255701, 2016.

[33] M. Kawakami, K. Byrne, B.S. Khatri, T. C. B. Mcleish, S. E. Radford, and D. A. Smith. Viscoelastic measurements of single molecules on a millisecond time scale by magnetically driven oscillation of an atomic force microscope cantilever. *Langmuir*, 21:4765–4772, 2005.

[34] A.D.L. Humphris, M. Antognozzi, T.J. McMaster, and M.J. Miles. Transverse dynamic force spectroscopy: A novel approach to determining the complex stiffness of a single molecule. *Langmuir*, 18:1729–1733, 2002.

[35] M. Doi and S.F. Edwards. *The Theory of Polymer Dynamics*. Oxford University Press, 1986.

[36] M. Doi and S.F. Edwards. *The Theory of Polymer Dynamics*, chapter 8, pages 295–296. Oxford University Press, 1986.

[37] Marshal Mandelkern, John G. Elias, Don Eden, and Donald M. Crothers. The dimensions of DNA in solution. *Journal of Molecular Biology*, 152(1):153–161, 1981.

[38] M. Doi and S.F. Edwards. *The Theory of Polymer Dynamics*, chapter 3, pages 56–58. Oxford University Press, 1986.

[39] Bhavin S. Khatri and Tom Charles Buckland McLeish. Rouse model with internal friction: A coarse grained framework for single biopolymer dynamics. *Macromolecules*, 40:6770 –6777, 2007.

[40] Christoph G. Baumann, Steven B. Smith, Victor A. Bloomfield, and Carlos Bustamante. Ionic effects on the elasticity of single DNA molecules. *Proceedings of the National Academy of Sciences*, 94(12):6185–6190, 1997.

[41] Huimin Chen, Steve P. Meisburger, Suzette A. Pabit, Julie L. Sutton, Watt W. Webb, and Lois Pollack. Ionic strength-dependent persistence lengths of single-stranded RNA and DNA. *Proceedings of the National Academy of Sciences*, 109(3):799–804, 2012.

[42] Sébastien Guilbaud, Laurence Salomé, Nicolas Destainville, Manoel Manghi, and Catherine Tardin. Dependence of DNA Persistence Length on Ionic Strength and Ion Type. *Physical Review Letters*, 122(2):028102, 2019.

[43] Jay R. Wenner, Mark C. Williams, Ioulia Rouzina, and Victor A. Bloomfield. Salt Dependence of the Elasticity and Overstretching Transition of Single DNA Molecules. *Biophysical Journal*, 82(6):3160–3169, 2002.

[44] Yeonee Seol, Jinyu Li, Philip C. Nelson, Thomas T. Perkins, and M.D. Betterton. Elasticity of Short DNA Molecules: Theory and Experiment for Contour Lengths of 0.6-7m. *Biophysical Journal*, 93(12):4360–4373, 2007.

[45] Paul A. Wiggins, Thijn van der Heijden, Fernando Moreno-Herrero, Andrew Spakowitz, Rob Phillips, Jonathan Widom, Cees Dekker, and Philip C. Nelson. High flexibility of DNA on short length scales probed by atomic force microscopy. *Nature Nanotechnology*, 1(2):137–141, 2006.

[46] Jiyoun Jeong and Harold D Kim. Determinants of cyclization-decyclization kinetics of short DNA with sticky ends. *Nucleic Acids Research*, 48(9):5147–5156, 2020.

[47] Hiromi Yamakawa and W H Stockmayer. Statistical Mechanics of Wormlike Chains. II. Excluded Volume Effects. *The Journal of Chemical Physics*, 57(7):2843–2854, 1972.

[48] J. F. Allemand, S. Cocco, N. Douarche, and G. Lia. Loops in DNA: An overview of experimental and theoretical approaches. *The European Physical Journal E*, 19(3):293–302, 2006.

[49] Aakash Basu, Dmitriy G. Bobrovnikov, Zan Qureshi, Tunc Kayikcioglu, Thuy T. M. Ngo, Anand Ranjan, Sebastian Eustermann, Basilio Cieza, Michael T. Morgan, Miroslav Hejna, H. Tomas Rube, Karl-Peter Hopfner, Cynthia Wolberger, Jun S. Song, and Taekjip Ha. Measuring DNA mechanics on the genome scale. *Nature*, 589(7842):462–467, 2021.

[50] Warren A. Whyte, David A. Orlando, Denes Hnisz, Brian J. Abraham, Charles Y. Lin, Michael H. Kagey, Peter B. Rahl, Tong Ihn Lee, and Richard A. Young. Master Transcription Factors and Mediator Establish Super-Enhancers at Key Cell Identity Genes. *Cell*, 153(2):307–319, 2013.

[51] Mahipal Ganji, Indra A. Shaltiel, Shveta Bisht, Eugene Kim, Ana Kalichava, Christian H. Haering, and Cees Dekker. Real-time imaging of DNA loop extrusion by condensin. *Science*, 360(6384):eaar7831, 2018.

[52] Michael G Poirier and John F Marko. Effect of internal friction on biofilament dynamics. *Physical review letters*, 88(22):228103, 2002.

[53] Tetsuya Hiraiwa and Takao Ohta. Linear viscoelasticity of a single semiflexible polymer with internal friction. *The Journal of chemical physics*, 133(4):044907, 2010.

[54] K. Berg-Sorensen and H. Flyvbjerg. Power spectrum analysis for optical tweezers. *Rev. Sci. Ins.*, 75:594–612, 2004.

Methods

Semiflexible polymer dynamics with bending friction

The standard approach to model the dynamics of locally stiff rod-like polymers, such as DNA is via a stochastic partial differential equation for the vectorial space curve $\boldsymbol{R}(s,t)$, which is a vector of the three dimensional position of the curve at a position s along the curve or backbone[52,53]. To incorporate the effect of intramolecular bending friction on the dynamics of DNA, we include dissipation proportional to the rate of change of local curvature of its backbone. This is described by the Rayleigh dissipation function $\mathcal{D} = \frac{1}{2}\zeta_B(\partial_t \partial_s^2 \boldsymbol{R})^2$, where ζ_B, is the bending friction constant. The local frictional forces due to bending dissipation are then calculated by a functional derivative of the dissipation function with respect to variation in the local velocity of the space curve, which gives rise to the following modified equation for semiflexible polymer dynamics (see Supplementary Information section S7 for details):

$$\tilde{\zeta}_s \frac{\partial \boldsymbol{R}(s,t)}{\partial t} + \zeta_B \frac{\partial}{\partial t}\frac{\partial^4 \boldsymbol{R}(s,t)}{\partial s^4} - F\frac{\partial^2 \boldsymbol{R}(s,t)}{\partial s^2} + \kappa_B \frac{\partial^4 \boldsymbol{R}(s,t)}{\partial s^4} = \boldsymbol{f}(s,t), \tag{4}$$

where $\tilde{\zeta}_s$ is a solvent friction per unit length, and $\kappa_B = k_B T \ell_p$ is the bending elastic constant and $\boldsymbol{f}(s,t)$ is a temporally white noise term, whose moments follow from the fluctuation dissipation theorem, but spatially coloured due the fact that dissipation occurs due to relative motion of adjacent points on the chain[39] (see Supplementary Information). Further, we have made the usual assumption at high stretch that $\boldsymbol{R}(s,t) \approx \boldsymbol{R}_\perp$, so that this equation only describes the dynamics of the transverse component of the space curve relative to the direction of the applied force F. Each term on the left-hand-side of this equation represents the force on an infinitesimal segment of the rod at position s along the backbone and at time t: the first is the force due solvent friction, the second — the new term for modelling DNA dynamics — the force due to bending friction, the third the external force, and the fourth the elastic forces.

Note that this equation ignores long range hydrodynamic interactions, which would give rise to Stoke's friction on the whole polymer scale, but is nonetheless reasonable when studying the internal dynamics of the polymer when highly stretched. It is for this reason that we treat the friction here as the excess friction due to bending dissipation and that we calculate from the data the equivalent quantity which effectively removes the contribution of DNA solvent friction (as well as the background bead friction), which will have a very weak and flat force dependence at high stretch ($F > 0.08$pN).

A normal mode analysis with wave number q_n, the relaxation time of mode number n is given by

$$\tau_n = \frac{\tilde{\zeta}_s + \zeta_B q_n^4}{\kappa_B q_n^4 + F q_n^2}, \tag{5}$$

which reflects the usual ratio of frictional to elastic forces for overdamped dynamics. We then have a set of stochastic differential equations describing the dynamics of each mode. The autocorrelation function of the chain end-to-end vector can be calculated by use of Wick's theorem[35] to evaluate the necessary 4th order moments between mode amplitudes. The end-to-end friction of the chain is then calculated from the derivative of the autocorrelation function evaluated with zero time lag[38]: $\frac{k_B T}{\zeta_{\Delta R}} = \left|\frac{\mathrm{d}\rho_{\Delta R}(t)}{\mathrm{d}t}\right|_{t=0}$ (or from the integral of the velocity autocorrelation function using the Green-Kubo theorem). Evaluating this then gives Eqn.1 in the main text.

DNA functionalisation

To facilitate attachment to beads, shorter DNA molecules (2.7 kbp and 4.5 kbp) were labelled with a single biotin and a single digoxigenin at either end of the DNA molecule. For longer molecules (6.5 kbp and 8.8 kbp) both DNA ends were labelled with biotins. Restriction enzymes, DNA polymerases and buffers were purchased from New England Biolabs (NEB). Oligonucleotides were purchased from Merck. All PCR reactions were performed using Phusion High-Fidelity DNA Polymerase in a Phusion HF Buffer (NEB).

2,655 bp biotin-digoxigenin DNA

2,655 bp DNA fragment was synthesised by PCR using Lambda-phage DNA (NEB) as a template, a 5'-biotin containing primer (LHD2_RT7bio) and a primer containing XbaI restriction site (LHD2_FXbaI). PCR reaction was purified using a PCR Cleanup Kit (Monarch T1030S, NEB) and the product was further digested with XbaI restriction enzyme (NEB) in a Standard Taq Reaction Buffer (NEB) for 40 minutes at 37 °C to generate a 4-nt single-stranded overhang. XbaI was inactivated by incubating the reaction for 20 minutes at 65 °C and the second end of the DNA was labelled with digoxigenin by end filling reaction using Taq DNA polymerase (NEB) and a mixture of dATP, dCTP, dGTP (Promega) and dUTP-digoxigenin (Jena Bioscience) performed for 30 min at 72 °C. The final product was purified using Micro Bio-Spin P30 spin column (Bio-Rad).

4,500 bp biotin-digoxigenin DNA

4,500 bp DNA fragment was synthesised by PCR using Lambda-phage DNA (NEB) as a template, a 5'-digoxigenin containing primer (LHT1_Fdig) and a 5'-biotin containing primer (4.5kb_rev_bio). PCR reaction was purified using a PCR Cleanup Kit (Monarch T1030S, NEB).

6,473 bp biotin-biotin DNA

9,847 bp plasmid DNA (8x601-pKYB1, a gift from Graeme King) was double digested with XbaI and SpeI restriction enzymes (NEB) for 1 hour at 37 °C in rCutSmart buffer (NEB), followed by inactivation for 20 minutes at 80 °C. This resulted in 2 fragments (6,473 bp and 3,374 bp long) containing 4-nt single-stranded ends. DNA ends were further biotinylated by addition of Klenow Fragment (3´→5´ exo-) of DNA Pol I (NEB), a mixture of dATP, dTTP, dGTP (Promega) and dCTP-biotin (Jena Bioscience) and incubation for 25 minutes at 37 °C, followed by inactivation for 20 minutes at 75 °C. DNA was cleaned-up from unincorporated nucleotides using Micro Bio-Spin P30 spin column (Bio-Rad). After tethering DNA to the beads only 6,473 bp-long molecules were selected by force-extension analysis.

8,815 bp biotin-biotin DNA

8,815 bp plasmid DNA (2x601-pKYB1, a gift from Graeme King) was digested with XbaI (NEB) in the Standard Taq Reaction Buffer (NEB) for 45 minutes at 37 °C to generate a 4-nt single-stranded overhangs. DNA ends were biotinylated by end filling reaction using Taq DNA polymerase (NEB) and a mixture of dATP, dTTP, dGTP (Promega) and dCTP-biotin (Jena Bioscience) performed for 30 min at 72 °C. The final product was purified using the Micro Bio-Spin P30 spin column (Bio-Rad).

4.5kb_rev_bio	Biotin-GTAAAAGCTCTTGGATTCCTGAAAC
LHT1_Fdig	Digoxigenin-CTGTTACAGGTCACTAATACCATC
LHD2_FXbaI	CACTCTAGAGTGTTTGATCCATTCTTTGGGAC
LHD2_RT7bio	Biotin-TAATACGACTCACTATAGGGTTTCCAGCATAAGCGGCTACATG

Table 1: List of oligonucleotides

Single-molecule DNA tethering

Experiments were performed using commercial dual-trap optical tweezers (C-trap, Lumicks) combined with a multi-channel microfluidic laminar flow cell (u-Flux, Lumicks). Before experiments, the flow cell was passivated by incubating it with 0.5% Pluronic F-127 (Merck) diluted in PBS (Phosphate Buffered Saline) for at least 30 minutes. Pluronic was washed by flowing at least 1 mL of PBS through each channel of the flow cell. Individual DNA molecules were tethered between 2 polystyrene beads of 2 μm diameter. Shorter digoxigenin-biotin labelled DNA molecules (2.7 and 4.5 kbp) were first coupled to Anti-digoxigenin-coated beads (DIGP-20-2, Spherotech): 5 microliters of beads stock solution (0.1% w/v) were gently mixed with 5 microliters of DNA diluted down to 30 pM in PBS and incubated for 10 min. The mixture was further diluted by adding 300 microliters of PBS and loaded into the first channel of the flow cell. The second channel was loaded with PBS and third channel contained Streptavidin-coated beads (SVP-20-5, Spherotech) diluted down to 0.002% w/v in PBS. 4th and 5th channels of the flow-cell contained a low salt buffer (Hepes pH 7.5 1mM, NaCl 1mM). To form a DNA tether, first a bead-DNA complex and a Streptavidin-coated bead were consecutively trapped in two optical traps in the first and the third channels respectively. The beads were further moved into the second channel where the free biotinylated end of DNA was attached to a Streptavidin-coated bead. The flow cell was extensively washed with PBS keeping only the 2nd channel open to remove any free-floating beads, after which the flow was stopped and measurements started. For longer biotinylated DNA molecules (6.5 and 8.8 kbp) the first channel contained Streptavidin-coated beads (SVP-20-5, Spherotech) diluted down to 0.002% w/v in PBS, second channel contained DNA diluted down to 5 pM in PBS, and the third channel was loaded with PBS. Two beads were trapped in the first channel and transferred into the second channel to form a DNA tether, which was further transferred into the 3rd channel and the flow was stopped prior to measurements. For measurements in the low salt buffer, after DNA fluctuations were measured in PBS, the 4th and 5th channels were extensively washed with the Hepes buffer (2 minutes at the pressure of 1 Bar). After this the flow was stopped and the DNA tether was transferred into the 5th channel where measurements were repeated. Not all DNA tethers lasted long enough to be measured in both PBS and Hepes buffers and hence in Table.2 the number of single molecules for PBS and Hepes differ for each length. After molecule detachment, time series of bead positions were collected at approximately the same trap separations as the force measurements with DNA.

Force-extension and force-dependent DNA fluctuation measurements

After the DNA tether was formed and placed in a channel containing either PBS or a low salt buffer, a force-extension curve was recorded by increasing the beads separation at the rate of 40 nm per second while simultaneously recording the distance between the beads and the force in the optical traps until the DNA tension reached 10 pN.

After that the DNA molecule was fully relaxed by bringing the beads closer to each other. Subsequently DNA was stretched to a required force and the fluctuations of each bead were

recorded simultaneously at $f_s = 78.125$kHz for a period of 6 seconds. These measurements were performed at DNA tensions varying between 1pN and 5pN with 0.5 pN incremental steps, with 3 repeats per each force.

Prior to the measurements the laser power was adjusted to reach the nominal trap stiffness of $\kappa_1 = \kappa_2 \approx 0.05$pN for each optical trap.

Data were acquired using a custom-made automation script. High-frequency force data and the distance between the beads measured at ≈ 50Hz were saved as an h5 file and further processed using Matlab.

The final numbers of molecules used for each length and each buffer condition are as in Table.2

Length	n
2.7kbp	(20,6)
4.5kbp	(21,18)
6.5kbp	(14,10)
8.8kbp	(13,8)

Table 2: Number of single molecules used at each length and each buffer condition. The first number in the brackets are the number of single molecules used in PBS buffer and the second number the number used in the Hepes buffer. Each single molecule experiment consisted of measurements in PBS followed by Hepes; however, the Hepes stage did not complete for all single molecules and so the 2nd number is typically less than the first.

For each single molecule experiment, we corrected forces according to Supplementary Information(section S6) to account for small positive forces — in the absence of DNA — between beads due to the cross-talk between traps at small trap separations.

Data processing

Raw data in the form of force signals from both traps were used to extract the DNA length fluctuations as follows: at each time point the length of the DNA molecule was calculated as

$$\ell(t) = D - 2b + x_2(t) - x_1(t) = \langle \ell \rangle + \frac{\langle F_1 \rangle + F_1(t)}{\kappa_1} + \frac{\langle F_2 \rangle - F_2(t)}{\kappa_2}$$

where D is the distance between trap centres, b the radius of each bead, $\langle F_2 \rangle = -\langle F_1 \rangle = F$ are the mean force in each trap averaged over the measurement period (6 seconds), where F is the magnitude of the desired force, κ_1, κ_2 are the trap stiffness values for trap 1 and trap 2, and are nominally equal and $\langle \ell \rangle$ is the mean DNA length, calculated as the distance between the beads averaged over the measurement period (6 seconds) with $2b$ subtracted, and F_1, and F_2 are the instantaneous forces on the beads in trap 1 and trap 2.

The power spectrum $P_\ell(\omega)$ of the time-series of DNA length $\ell(t)$ is then calculated by standard Fast Fourier Transform (FFT) in MatLab,

$$P_\ell(\omega) = \frac{1}{T}\mathrm{FFT}\{\ell(t)\} \times \mathrm{FFT}^*\{\ell(t)\}$$

where * indicates complex conjugate and $T = 5000$msec is the maximum observation time in the data. The power spectrum is then block-averaged on a log-frequency scale[54] with $n = 25$ blocks, to reduce the noise on the raw power spectrum estimate. The zero-frequency (DC) component is removed and only frequencies less than the Nyquist frequency ($f_s/2$) are retained. The velocity power spectrum is then calculated by $P_v(\omega) = \omega^2 P_\ell(\omega)$.

As described in the main text, the velocity power spectrum is then fit with Eqn.S18 (Supplementary Information) at each force F to obtain $\zeta(F)$, $\kappa(F)$ and $m_{eff}(F)$.

Data Availability

Sample data is available with the code (see code availability) and data used to plot all figures will be made available at the time of publication. The rest of raw data is available from the corresponding authors upon request.

Code availability

We provide example code with an example data set of a single molecule of 2.7kbp long DNA to calculate and plot the results of Fig.2c&d (the velocity power spectrum and total friction as a function of force). Code used to plot all figures will be made available at the time of publication.

Acknowledgements

BSK would like to thank the Isaac Newton Institute for Mathematical Sciences, Cambridge, for support and hospitality during the programme "New statistical physics in living matter: non equilibrium states under adaptive control", where part of the work on this paper was undertaken. This work was supported by EPSRC grant EP/R014604/1. GP and MM are supported by the Francis Crick Institute, which received funding from the UK Medical Research Council (FC001750), Cancer Research UK (FC001750) and the Wellcome Trust (FC001750) through "Mechanobiology and biophysics" award to MM. We would also like to thank Frank Uhlmann, Ard Louis, Agnes Noy, and Tanniemola Liverpool for various discussions and suggestions on the text and figures of the manuscript. We thank Holly Folkard-Tapp for her advice on the design of the graphical elements.

Competing interests

The author declares that they have no competing interests.